HAL
open science

IRSBOT-2: A Novel Two-Dof Parallel Robot for High-Speed Operations

Coralie Germain, Sébastien Briot, Victor Glazunov, Stéphane Caro, Philippe Wenger

To cite this version:

Coralie Germain, Sébastien Briot, Victor Glazunov, Stéphane Caro, Philippe Wenger. IRSBOT-2: A Novel Two-Dof Parallel Robot for High-Speed Operations. ASME 2011 International Design Engineering Technical Conferences & Computers and Information in Engineering Conference IDETC/CIE 2011, Aug 2011, Washington, United States. 10.1115/DETC2011-47564 . hal-00590082

HAL Id: hal-00590082

https://hal.science/hal-00590082

Submitted on 3 Feb 2019

HAL is a multi-disciplinary open access archive for the deposit and dissemination of scientific research documents, whether they are published or not. The documents may come from teaching and research institutions in France or abroad, or from public or private research centers.

L'archive ouverte pluridisciplinaire **HAL**, est destinée au dépôt et à la diffusion de documents scientifiques de niveau recherche, publiés ou non, émanant des établissements d'enseignement et de recherche français ou étrangers, des laboratoires publics ou privés.

the ASME 2011 International Design Engineering Technical Conferences &
Computers and Information in Engineering Conference
IDETC/CIE 2011
August 29-312011Washington, DCUSA

DETC2011/47564

IRSBOT-2: A NOVEL TWO-DOF PARALLEL ROBOT FOR HIGH-SPEED OPERATIONS

Coralie Germain†, **Sébastien Briot**†, **Victor Glazunov**⋆, **Stéphane Caro**†, **Philippe Wenger**†
† Institut de Recherche en Communications et Cybernétique de Nantes, UMR CNRS n° 6597
1 rue de la Noë, 44321 Nantes, France
⋆ Mechanical Engineering Research Institute, Russian Academy of Sciences
M.Kharitonyevski Str. 4, 101990 Moscow, Russia
Email: {germain, briot, caro, wenger}@irccyn.ec-nantes.fr, vaglznv@mail.ru

ABSTRACT

*This paper presents a novel two-degree-of-freedom (DOF) translational parallel robot for high-speed applications named the IRSBot-2 (acronym for **IR**CCyN **S**patial Ro**bot** with **2** DOF). Unlike most two-DOF robots dedicated to planar translational motions, this robot has two spatial kinematic chains which confers a very good intrinsic stiffness. First, the robot architecture is described. Then, its actuation and constraint singularities are analyzed. Finally, the IRSBot-2 is compared to its two-DOF counterparts based on elastostatic performances.*

INTRODUCTION

Since the creation of the Delta robot [1, 2], parallel robots are increasingly used in industry, especially for Pick-and-Place operations.

Several robot architectures for high-speed operations have been proposed in the past decades [1–16]. Many of them have four degrees of freedom (DOF): three translations and one rotation about a fixed axis (Schoenflies motions [17]). Nevertheless, some simple operations need only two translational DOF in order to transfer a part from a working area to another (e.g. conveyors). Therefore, several robot architectures with two translational DOF have been proposed. Among them, those that have the capacity to fix the orientation of the platform via the use of a planar parallelogram (also called a Π joint) are necessary in numerous operations. For example, Brogårdh proposed in [14] an architecture made of a Π linkage located between the linear actuators and the platform. A version of this robot actuated with revolute joints, is commercialized by Elau [6]. Another 2-DOF translational robot was presented in [15], where the authors use two Π linkages to join the platform with two vertical prismatic actuators. Its equivalent architecture actuated by revolute joints is presented in [16]. The main common point between these architectures is that they are all planar, i.e. all their elements are constrained to move in the plane of the motion. As a result, all their elements are subject to bending effects in the direction normal to the plane of motion. In order to guarantee a minimum stiffness in this direction, the elements have to be bulky, leading to high inertia and to low acceleration capacities. In order to overcome these problems, the authors of [18] have recently proposed a new Delta-like robot named the Par2 (Fig. 1). This robot has the following properties: all the elements of the distal parts of the legs are only subject to traction/compression effects. This leads to a lighter structure with better acceleration capacities. The authors successfully built a prototype that can reach 53 G. However, even if its acceleration capacities are impressive, its accuracy is poor. This phenomenon can be explained by the complexity of the architecture composed of four identical legs among which two of them are linked by a rigid belt in order to constrain the motion of the moving-platform. As a result, this robot is more subject to parasitic effects that are difficult to identify and can decrease its accuracy. Moreover, its Cartesian workspace is rather small because the robot has four legs.

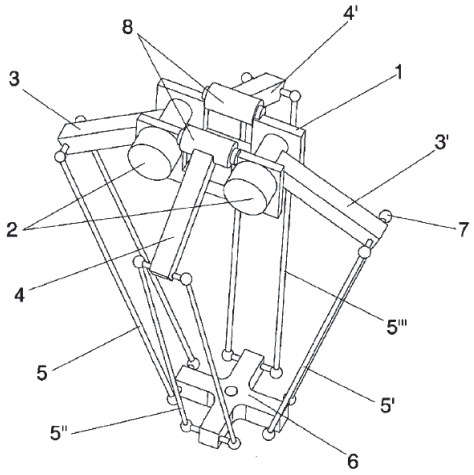

FIGURE 1. SCHEMATICS OF THE PAR2 ROBOT (COURTESY OF THE LIRMM) [18].

Accordingly, this paper introduces a novel two-DOF translational robot, named IRSBot-2, to overcome its counterparts in terms of mass in motion, stiffness and workspace size. IRSBot-2 stands for "**IR**CCyN **S**patial Ro**bot** with **2** DOF" and has the following characteristics:

(i) Like the Par2, it has a spatial architecture in which the distal parts of the legs are subject to traction/compression/torsion only. As a result, its stiffness is increased and its total mass can be reduced
(ii) It is composed of only two legs in order to reduce the mechanism complexity and to increase the size of its Cartesian workspace

The paper is organized as follows. First the robot architecture is described. Then, its geometric and kinematic models are written and its actuation and constraint singularities are analyzed. Finally, the IRSBot-2 is compared to its two-DOF counterparts based on the mass in motion and stiffness.

ROBOT ARCHITECTURE

The IRSBot-2 is a new parallel robot with two translational degrees of freedom along the $\mathbf{x}_0$ and $\mathbf{z}_0$ axes of the frame depicted in Fig. 2. It is made of two identical legs linking the fixed base and the moving platform.

Each leg is composed of a proximal module and a distal module. The proximal module is achieved through the use of a planar parallelogram linkage, also called Π joint, formed by the elements 0_i, 1_i, 2_i and 3_i ($i = 1, 2$) of axis $\mathbf{y}_0$. The parallelogram aims to keep the planes $\mathscr{P}_0$ and $\mathscr{P}_1$ parallel. The global frame $(\mathbf{x_0}, \mathbf{y_0}, \mathbf{z_0})$ is attached to the plane $\mathscr{P}_0$.

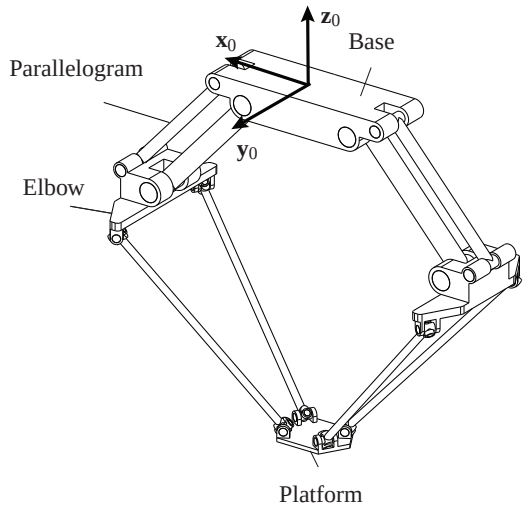

(a) CAO MODELLING.

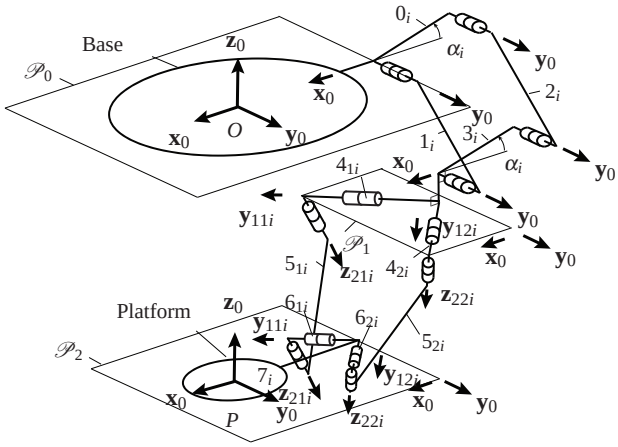

(b) KINEMATICS CHAIN OF i-TH LEG ($i = 1, 2$).

FIGURE 2. SCHEMATIC REPRESENTATION OF IRSBOT-2.

Unlike classical planar robots, the distal module elements do not move in parallel planes. However, the moving platform is constrained to move in the vertical plane $(\mathbf{x}_0, O, \mathbf{z}_0)$.

The distal module is attached to (i) the element 3_i of the parallelogram with two revolute joints of axis $\mathbf{y_{1}}_{ji}$ lying in the plane $\mathscr{P}_1$ and (ii) to the element 7_i of the moving platform with two revolute joints of axis $\mathbf{y_{1}}_{ji}$ lying in the plane $\mathscr{P}_2$ ($j = 1, 2$). Planes $\mathscr{P}_1$ and $\mathscr{P}_2$ are parallel, so $\mathscr{P}_2$ is parallel to $\mathscr{P}_0$. The axes $\mathbf{y_{11}}_i$ and $\mathbf{y_{12}}_i$ (resp. $\mathbf{z_{21}}_i$ and $\mathbf{z_{22}}_i$) are built symmetrically about the plane $(\mathbf{x}_0, O, \mathbf{z}_0)$. We can notice that elements 5_{1i} and 5_{2i} are not parallel, otherwise the distal module would become a spatial parallelogram and the robot architecture would be singular.

The distal module may be decomposed into two identical parts, composed of elements 4_{ji}, 5_{ji} et 6_{ji} ($j = 1, 2$). These elements are linked together by revolute joints of axes $\mathbf{z_{2}}_{ji}$. It should be mentioned that the axes $\mathbf{y_{1}}_{ji}$ and $\mathbf{z_{2}}_{ji}$ are orthogonal.

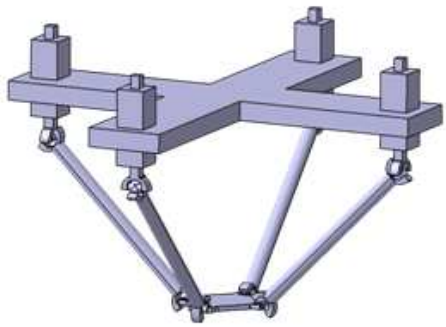

(a) 3D MODELLING.

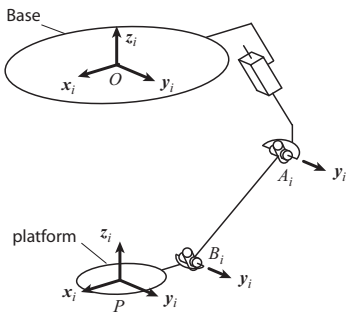

(b) SCHEMATICS OF i-TH LEG.

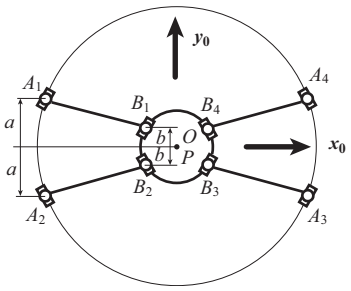

(c) TOP VIEW IN THE HOME CONFIGURATION.

FIGURE 3. KINEMATIC ARCHITECTURE OF THE REDUNDANT DELTA ROBOT.

For a better understanding of the IRSBot-2 mobility, let us consider the robot depicted in Fig. 3. It is a linear Delta robot composed of four identical legs linking the base and the platform. Each leg is actuated by one prismatic pair connected to link A_iB_i with a universal joint. The other end of link A_iB_i is connected to the platform with another universal joint. The robot is redundant because it has four actuators and its moving platform generates three translational degree-of-freedom motions.

In order for the moving platform of the robot to admit a translation movement only in the plane $(\mathbf{x_0}, O, \mathbf{z_0})$ containing the base center O (Fig. 3(c)), the centers of the universal joints A_i

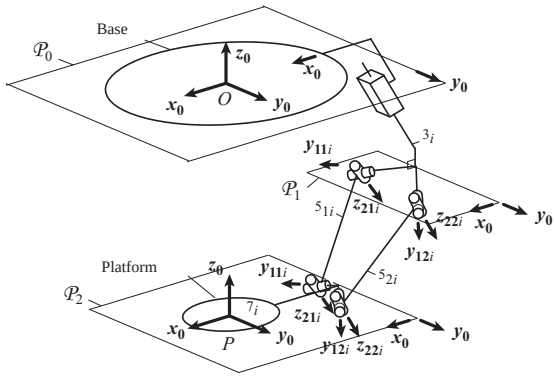

FIGURE 4. SCHEMATICS OF i-TH LEG OF THE IRSBOT-2 WHEN THE Π JOINT IS REPLACED BY A PRISMATIC JOINT.

$(i = 1 \ldots 4)$ of the first and second legs on the one hand, and of the third and fourth legs on the other hand, must have the same Z-coordinate, i.e. $z_{A_1} = z_{A_2}$ and $z_{A_3} = z_{A_4}$, where z_{A_i} denotes the Cartesian coordinate of point A_i along $\mathbf{z}_0$. Accordingly, a solution for the centers of the universal joints of legs 1 and 2 (resp. 3 and 4) to keep the same Z-coordinate is to link them to the same actuator. This solution is illustrated in Fig. 4. Note that if the prismatic joints is replaced by Π joints, then this architecture will be equivalent to the one shown in Fig. 2.

Advantages of the new architecture

The advantages of such a robot are the following :

- as compared to planar architectures with 2-translational DOF robots for which each element is subject to bending constraints along the axis orthogonal to the plane of the movement, the elements 5_{ji} of IRSBot-2 are only subject to traction/compression/torsion constraints. For the IRSBot-2 robot, all the flexion constraints are moved into the parallelogram, which increases the intrinsic stiffness of the architecture. Its dynamical performances can be improved by decreasing its mass and its precision can be improved by reducing the bending of its elements.
- as compared to the Par2 robot [19], the only spatial-architecture robot with 2-translational DOF that can be found in the literature, the IRSBot-2 (i) is simpler, and therefore less subject to uncontrolled parasitic effects, and (ii) has a larger workspace, since it has only two legs.

KINEMATIC AND VELOCITY MODELS

The parameters used to define the kinematic model of the IRSBot-2 robot are depicted in Fig. 5. Let q_i be the actuated joint coordinate of the i-th leg $(i = 1, 2)$, $b = OA_i$ the radius of the base, $l_1 = A_iB_i$ the length of the proximal legs, $l_2 = E_{ji}F_{ji}$ the length of the spatial distal legs, a_1 and a_2 denote the lengths

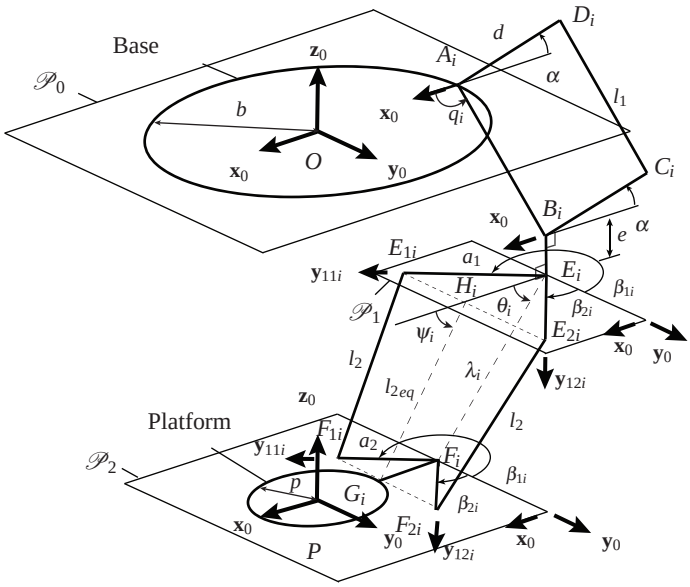

FIGURE 5. PARAMETRIZATION OF THE MECHANISM.

of E_iE_{ji} and F_iF_{ji}, respectively. One can notice that the angle between E_iE_{ji} and $\mathbf{y}_0$ (resp. F_iF_{ji} and $\mathbf{y}_0$) is constant and is equals to β_{ji}[1]. Points H_i and G_i are defined as the midpoints of $E_{1i}E_{2i}$ and $F_{1i}F_{2i}$, respectively. By construction, H_i lies in plane $\mathscr{P}_1$ and G_i in plane $\mathscr{P}_2$. From the Pythagorean theorem, the length between points H_i and G_i is constant and equal to

$$l_{2eq} = \sqrt{l_2^2 - (a_1 - a_2)^2 \cos\beta^2}. \tag{1}$$

Let ψ_i be the angle between axis $\mathbf{x}_0$ and the line defined by H_iG_i. Finally, $p = PG_i$ is the radius of the platform and e is an offset along $\mathbf{z}_0$ between the proximal and distal modules.

The loop closure equation is (for $i = 1, 2$):

$$\overrightarrow{OP} = \overrightarrow{OA_i} + \overrightarrow{A_iB_i} + \overrightarrow{B_iE_i} + \overrightarrow{E_iH_i} + \overrightarrow{H_iG_i} + \overrightarrow{G_iP} \tag{2}$$

which yields after simplifications:

$$l_{2eq}\cos\psi_i = x + \sigma_i b_0 - l_1 \cos q_i \tag{3a}$$
$$-l_{2eq}\sin\psi_i = z + e + l_1 \sin q_i \tag{3b}$$

with $b_0 = b - p - a_1 \sin\beta$ and $\sigma_i = (-1)^{i-1}$.
Squaring (3a) and (3b) and summing leads to

$$l_{2eq}^2 = (x + \sigma_i b_0 - l_1 \cos q_i)^2 + (z + l_1 \sin q_i + e)^2 \tag{4}$$

[1]Let β denote $\beta_{22} = \beta$, then $\beta_{11} = \pi + \beta$, $\beta_{21} = -\beta$ and $\beta_{12} = \pi - \beta$

In this expression, it should be mentioned that the terms "$-p + a_1 \sin\beta$" (contained in b_0) and "e" are constant. In case they vanish, Eqn. (4) is equivalent to the loop closure equation of a $\underline{R}RRRR\underline{R}$[2] mechanism [20], l_1 being the length of the proximal bars, l_{2eq} the length of the distal bars, and $2b$ the distance between the axes of the two actuated joints. Hence, one can solve the direct and inverse kinematic problem of the IRSBot-2 similarly to $\underline{R}RRRR\underline{R}$ mechanism [20].

The inverse kinematic model (IKM) is expressed as follow:

$$q_i = 2\tan^{-1}\frac{-B_i \pm \sqrt{B_i^2 + A_i^2 - C_i^2}}{C_i - A_i}, \; i = 1, 2, \tag{5a}$$
$$A_i = -2l_1(x + \sigma_i b_0) \tag{5b}$$
$$B_i = 2l_1(z + e) \tag{5c}$$
$$C_i = (x + \sigma_i b_0)^2 + (z + e)^2 + l_1^2 - l_{2eq}^2 \tag{5d}$$

The sign $\pm$ corresponds to the four working modes of the robot [21].

The direct kinematic model (DGM) is expressed as follow:

$$x = \frac{c_2 - c_1 - 2z(a_{z1} - a_{z2})}{2(a_{x1} - a_{x2})} \text{ et } z = \frac{-h \pm \sqrt{h^2 - jg}}{g} \tag{6a}$$

with

$$a_{xi} = \sigma_i b_0 - l_1 \cos q_i \tag{6b}$$
$$a_{zi} = l_1 \sin q_i + e \tag{6c}$$
$$c_i = a_{xi}^2 + a_{zi}^2 - l_{2eq}^2 \tag{6d}$$
$$j = c_1 + \frac{(c_2 - c_1)^2}{4(a_{x1} - a_{x2})^2} + \frac{a_{x1}(c_2 - c_1)}{a_{x1} - a_{x2}} \tag{6e}$$
$$g = 1 + \frac{(a_{z1} - a_{z2})^2}{(a_{x1} - a_{x2})^2} \tag{6f}$$
$$h = \frac{(c_2 - c_1)(a_{z1} - a_{z2})}{2(a_{x1} - a_{x2})} + \frac{a_{x1}(a_{z1} - a_{z2})}{a_{x1} - a_{x2}} \tag{6g}$$

The sign $\pm$ corresponds to the two assembly modes of the robot [21].

The velocity model is obtained by differentiating the loop closure equation (4) with respect to time:

$$\mathbf{A}\mathbf{t} + \mathbf{B}\dot{\mathbf{q}} = 0, \tag{7a}$$

[2]In the remainder of the paper, R stands for a passive revolute joint and $\underline{R}$ for an active revolute joint.

with

$$\mathbf{B} = \begin{bmatrix} 2l_{2eq}l_1\sin(q_1-\psi_1) & 0 \\ 0 & 2l_{2eq}l_1\sin(q_2-\psi_2) \end{bmatrix} \tag{7b}$$

$$\mathbf{A} = \begin{bmatrix} 2l_{2eq}\cos\psi_1 & 2l_{2eq}\sin\psi_1 \\ 2l_{2eq}\cos\psi_2 & 2l_{2eq}\sin\psi_2 \end{bmatrix} \tag{7c}$$

where $$\psi_i = \tan^{-1}\frac{z+l_1\sin q_i+e}{x+\sigma_i b_0 - l_1\cos q_i} \tag{7d}$$

$\mathbf{A}$ and $\mathbf{B}$ are respectively the Type 1 and Type 2 Jacobian matrices [22], $\dot{\mathbf{q}} = [\dot{q}_1\ \dot{q}_2]^T$ is the joint rates vector and $\mathbf{t} = [\dot{x}\ \dot{z}]^T$ is the twist of the moving platform. Let us recall that ψ_i is the angle between $\mathbf{x}_0$ and line H_iG_i.

SINGULARITY ANALYSIS

The main three types of singularities [22] can be determined from Eqn. (7a).

1. if $\det(\mathbf{B}) = 0$, the robot loses one or more DOF and reaches a Type 1 singularity
2. if $\det(\mathbf{A}) = 0$, the robot gains one or more uncontrolled DOF and reaches a Type 2 singularity
3. if $\det(\mathbf{A}) = \det(\mathbf{B}) = 0$, the robot reaches a Type 3 singularity. In the following, we only focus on the analysis of Type 1 and Type 2 singularities, since Type 3 singularities are obtained from the two previous types.

Like for a $\underline{R}RRR\underline{R}$ mechanism, it is possible to show that the Type 1 singularities arise in the configurations where segments $[A_iB_i]$ and $[H_iG_i]$ are parallel (Fig. 6(a)), i.e. $q_i = \psi_i + k\pi$, with $k \in \mathbb{Z}$. Such configurations correspond to the boundaries of the Cartesian workspace [23].

The Type 2 singularities arise when segments $[H_1G_1]$ and $[H_2G_2]$ are parallel (Fig. 6(b)), i.e. $\psi_1 = \psi_2 + k\pi$, with $k \in \mathbb{Z}$. In such configurations, the displacement of the end effector along the normal to the distal legs and in the plane $(\mathbf{x}_0, O, \mathbf{z}_0)$ is no longer controlled.

Since the robot has less than six DOF, it may also have constraint singularities [24]. Such singularities arise when the wrench system composed of all the constraints applied to the platform degenerates. In these configurations, the moving platform is not constrained to have a translational motion in plane $(\mathbf{x}_0, O, \mathbf{z}_0)$ anymore and the mechanism gains one or more DOF. The constraint singularities are analyzed below.

Constraint singularity analysis using screw theory

This section aims to determine the constraint singularities of the IRSBot-2 using screw theory. Each leg of the IRSBot-2 robot can be decomposed into two closed kinematic chains: the parallelogram and the spatial distal parts. We first need to find the equivalent twist of each part, then find the equivalent twist of each leg of the robot. Finally, we analyse the linear dependence of the complete equivalent screw system.

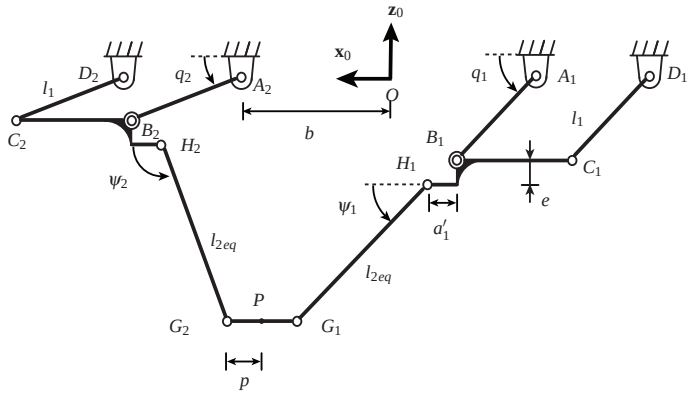

(a) IRSBOT-2 IN A TYPE 1 SINGULARITY

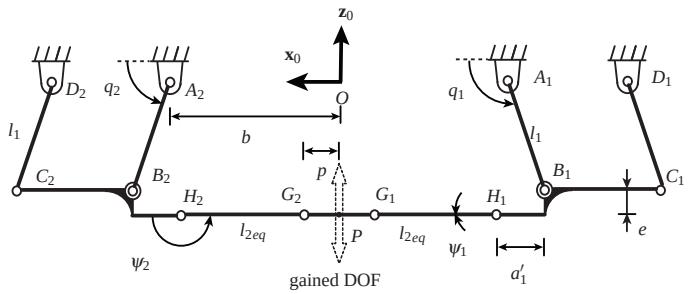

(b) IRSBOT-2 IN A TYPE 2 SINGULARITY

FIGURE 6. EQUIVALENT SCHEME OF THE IRSBOT-2 IN THE PLANE $(\mathbf{x}_0, O, \mathbf{z}_0)$ IN SINGULAR CONFIGURATIONS WHERE $a'_1 = a_1\sin\beta$.

It is possible to show that the displacement of the parallelogram can be identified with the displacement created by an infinite-pitch twist $\mathscr{W}_{pi}$ corresponding to the prismatic joint along the direction orthogonal to (A_iB_i), i.e., $\mathscr{W}_{pi} = (0,\ 0,\ 0,\ w^{\circ}_{pi_x},\ 0,\ w^{\circ}_{pi_z})$ [25] (Fig. 7(a)).

For the distal module, we need to decompose the problem into two subchains. First, one can find the reciprocal wrench of the unit twist of each kinematic subchain only composed of the elements 4_{ji}, 5_{ji} and 6_{ji}. These wrenches are denoted $\mathscr{R}_{1j}$ and $\mathscr{R}_{2j}$ for each subchain j. Hence, each distal module admits a wrench system $\{\mathscr{R}_{11},\ \mathscr{R}_{21},\ \mathscr{R}_{12},\ \mathscr{R}_{22}\}$. The reciprocal twist of the above system describes the motion allowed by the distal module. These twists, denoted by $\mathscr{W}_{1i}$ and $\mathscr{W}_{2i}$ are depicted in Fig. 7(b). $\mathscr{W}_{1i}$ is an infinite pitch twist, $\mathscr{W}_{1i} = (0,\ 0,\ 0,\ w^{\circ}_{1i_x},\ 0,\ w^{\circ}_{1i_z})$, and $\mathscr{W}_{2i}$ is a zero pitch twist, i.e., $\mathscr{W}_{2i} = (w_{2i_x},\ 0,\ w_{2i_z},\ 0,\ w^{\circ}_{2i_y},\ 0)$.

It should be mentioned that all the axes of the equivalent twists each leg of the IRSBot-2 lie in the plane of motion

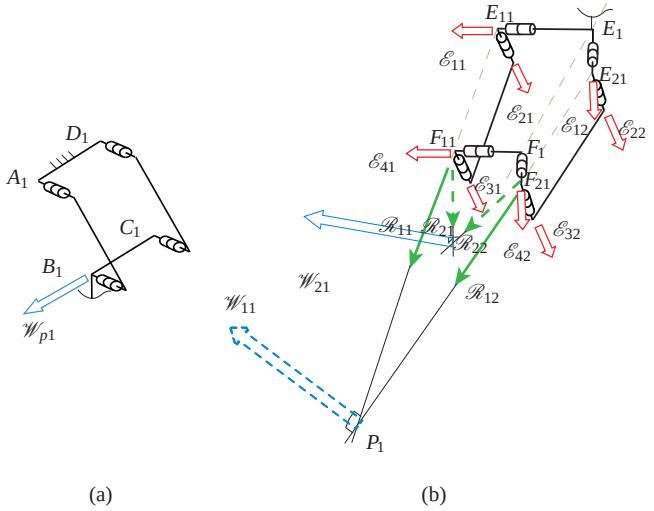

FIGURE 7. EQUIVALENT TWIST OF: (a) THE PROXIMAL LINK AND (b) THE DISTAL LINK. THE TWISTS AND THE WRENCHES ARE REPRESENTED BY DOUBLE AND SINGLE ARROWS, RESP. THE ZERO-PITCH AND INFINITE-PITCH SCREWS ARE REPRESENTED BY CONTINUOUS AND DASHED LINES, RESP.

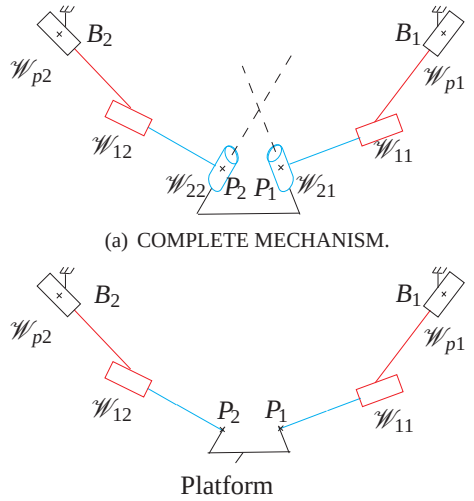

(a) COMPLETE MECHANISM.

(b) IF THE AXES OF REVOLUTE JOINTS MAKE THE SUB-SYSTEM REVOLUTE JOINTS + PLATFORM BLOCKED.

FIGURE 8. INSTANTANEOUS TWIST REPRESENTATION OF THE IRSBOT-2.

$(\mathbf{x}_0, O, \mathbf{z}_0)$ of the end-effector. As a consequence, the IRSBot-2 is equivalent, in terms of its instantaneous motions, to the planar mechanism shown in Fig. 8(a). Looking at the subsystem only composed of the two revolute joints and the platform, it should be noticed that it cannot move as long as the axes of the two virtual revolute joints intersect at a unique point. In this case, the mechanism depicted in Fig. 8(a) can be replaced by the one shown in Fig. 8(b) that does not have any constraint singularity. Therefore, constraint singularities appear if and only if the system formed by the twists $\mathscr{W}_{21}$ et $\mathscr{W}_{22}$ degenerates, i.e., if these twists are aligned (Fig. 9).

As shown in [26], the expressions of twists $\mathscr{W}_{21}$ and $\mathscr{W}_{21}$ in P_1 are given by:

$$\mathscr{W}_{2i} = (\sin\theta_i,\ 0,\ \cos\beta^2\cos\theta_i,\ 0,\ w^{\circ}_{2i_y},\ 0)\ ,\ i = 1, 2 \tag{8a}$$

with

$$w^{\circ}_{21_y} = 0 \tag{8b}$$

$$w^{\circ}_{22_y} = (x_{P_2} - x_{P_1})\cos\beta^2\cos\theta_2 - (z_{P_2} - z_{P_1})\sin\theta_2 \tag{8c}$$

where θ_i is the angle between the axis $\mathbf{x}_0$ end the line E_iF_i (Fig. 5).

Hence, the system composed by the twists $\mathscr{W}_{21}$ and $\mathscr{W}_{22}$ degenerates if and only if

$$\theta_1 = \theta_2 + k\pi,\ k = 0, 1 \tag{9}$$

$$w^{\circ}_{22_y} = (x_{P_2} - x_{P_1})\cos\beta^2\cos\theta_2 - (z_{P_2} - z_{P_1})\sin\theta_2 = 0 \tag{10}$$

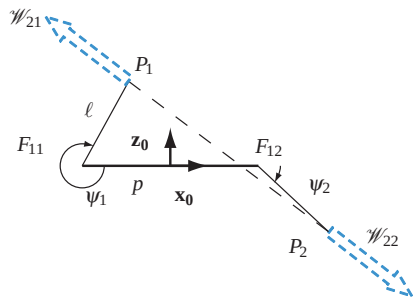

FIGURE 9. TWISTS $\mathscr{W}_{21}$ AND $\mathscr{W}_{22}$ FOR A CONSTRAINT SINGULARITY CONFIGURATION IN THE PLANE $(\mathbf{x}_0, O, \mathbf{z}_0)$.

It was shown in [26] that the manipulator does not reach any constraint singularity throughout its Cartesian Workspace for some design parameters.

PERFORMANCE ANALYSIS OF THE IRSBOT-2

The subject of this section is about the comparison of the IRSBot-2 with its counterparts. In this vein, we use the approach outlined in [19] that aims to compare the $\underline{R}RRR\underline{R}$ and the Par2 robots in terms of mass and stiffness. In [19], the authors show that for a given set of design parameters, the Par2 robot in its home configuration is lighter and stiffer along the normal to the plane of the moving platform than the $\underline{R}RRR\underline{R}$ robot. Here, a similar comparative study is done between the IRSBot-2, the Par2 and the $\underline{R}RRR\underline{R}$ robots.

Stiffness modelling

As these three robots are compared based on their stiffness, it is necessary to determine their stiffness model. The approach used is outlined in [27]. Each link of the robot is replaced by a rigid element followed by a localized spring that describes both the linear/rotational deflection of the links and the coupling between them.

According to [27], the small displacement screw of the end-effector $\delta\mathbf{t}_i$ of the i-th leg is related to the external force $\mathbf{f}$ applied to the end-effector by the following relationship:

$$\begin{bmatrix} \mathbf{S}_\theta^i & \mathbf{J}_q^i \\ \mathbf{J}_q^{i\,T} & 0 \end{bmatrix} \begin{bmatrix} \mathbf{f} \\ \delta\mathbf{q}_i \end{bmatrix} = \begin{bmatrix} \delta\mathbf{t}_i \\ 0 \end{bmatrix}, \mathbf{S}_\theta^{\mathbf{i}} = \mathbf{J}_\theta^i \mathbf{K}_\theta^{i\,-1} \mathbf{J}_\theta^{i\,T} \tag{11}$$

where vector $\delta\mathbf{q}_i$ includes the small passive joint displacements, $\mathbf{K}_\theta^i$ is a matrix including on its diagonal the aggregated spring stiffness of each virtual spring of the i-th leg. $\mathbf{J}_\theta^i$, $\mathbf{J}_q^i$ are the Jacobian matrices relating the small displacement screw of the end-effector $\delta\mathbf{t}_i$ of the i-th leg, to the vector $\delta\boldsymbol{\theta}_i$ collecting all virtual joint deflections, and to the vector $\delta\mathbf{q}_i$ collecting all small passive joint displacements is such as

$$\delta\mathbf{t}_i = \mathbf{J}_q^i \delta\mathbf{q}_i + \mathbf{J}_\theta^i \delta\boldsymbol{\theta}_i, \mathbf{J}_\theta^i = \left[\frac{\partial\mathbf{t}_i}{\partial\boldsymbol{\theta}_i}\right], \mathbf{J}_q^i = \left[\frac{\partial\mathbf{t}_i}{\partial\mathbf{q}_i}\right] \tag{12}$$

The equivalent stiffness matrix $\mathbf{K}_i$ of the i-th leg is obtained by direct inversion of relevant matrix in the left-hand side of (11). The stiffness matrix of the entire robot is obtained by summing the stiffness matrix of each leg:

$$\mathbf{K} = \sum_{i=1}^{n} \mathbf{K}_i \tag{13}$$

where n is the number of legs of the robot under study.

In the remainder, the proposed methodology is only detailed for the IRSBot-2 robot. The moving platform is assumed to be rigid. It should be noticed that each leg of the IRSBot-2 is composed of two closed kinematic chains, therefore it is necessary to find the stiffness matrix of each sub-chain. $\mathbf{K}_{\text{para}}^i$ denotes the stiffness matrix of the kinematic chain constituting the parallelogram linkage of the i-th leg and $\mathbf{K}_{\text{sp}}^i$ denotes the stiffness matrix of the spatial distal module.

The elastostatic model of the parallelogram and its stiffness matrix $\mathbf{K}_{\text{para}}$ are not detailed in this paper, they can be found in [27] and [28]. However, it is necessary to determine the flexible model of the spatial distal module to obtain its equivalent stiffness matrix.

The spatial distal module i can be decomposed into two identical kinematic sub-chains ji (Fig. 10) linking the elbow to the platform. Each sub-chain can be described by a serial structure that includes sequentially:

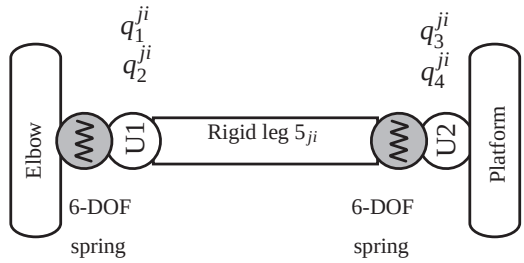

FIGURE 10. ELASTOSTATIC MODEL OF THE SPATIAL DISTAL MODULE ji.

(a) a rigid link corresponding to the elbow, i.e., the element 4_{ji} (Fig. 5), described by the constant homogeneous transformation matrix $\mathbf{T}_{\text{base-elbow}}^{ji}$;
(b) a 6-DOF spring describing the elbow stiffness, which is defined by the homogeneous transformation matrix function $\mathbf{V}_s(\theta_0^{ji},\ldots,\theta_5^{ji})$, where $\{\theta_0^{ji},\theta_1^{ji},\theta_2^{ji}\},\{\theta_3^{ji},\theta_4^{ji},\theta_5^{ji}\}$ are the virtual spring coordinates corresponding to the spring translational and rotational deflections;
(c) a 2-DOF passive U-joint at the beginning of the leg allowing two independent rotations of angles q_1^{ji} about $\mathbf{y}_{1ji}$ and q_2^{ji} about $\mathbf{z}_{2ji}$, which is described by the homogeneous transformation matrix function $\mathbf{V}_{r1,r2}(q_1^{ji},q_2^{ji})$;
(d) a rigid "leg" linking the elbow to the mobile platform, which is described by the constant homogeneous transformation matrix $\mathbf{T}_{\text{leg}}^{ji}$;
(e) a 6-DOF spring describing the leg stiffness, which is defined by the homogeneous transformation matrix function $\mathbf{V}_s(\theta_6^{ji},\ldots,\theta_{11}^{ji})$, where $\{\theta_6^{ji},\theta_7^{ji},\theta_8^{ji}\},\{\theta_9^{ji},\theta_{10}^{ji},\theta_{11}^{ji}\}$ correspond to the spring translations and rotations;
(f) a 2-DOF passive U-joint at the end of the leg allowing two independent rotations of angles q_3^{ji} about $\mathbf{y}_{1ji}$ and q_4^{ji} about $\mathbf{z}_{2ji}$, which is described by the homogeneous transformation matrix function $\mathbf{V}_{r3,r4}(q_3^{ji},q_4^{ji})$;
(g) a rigid link from the robot leg to the end-effector described by the constant homogeneous transformation matrix $\mathbf{T}_{\text{tool-spa}}^{ji}$

The global homogeneous transformation matrix describing the end-effector location from the elbow of a single kinematic chain ji may be written as follows:

$$\begin{aligned}\mathbf{T}_{\text{chain}}^{ji} =& \mathbf{T}_{\text{base-elbow}}^{ji}\mathbf{V}_s(\theta_0^{ji},\ldots,\theta_5^{ij})\mathbf{V}_{r1,r2}(q_1^{ji},q_2^{ji}) \\ & \mathbf{T}_{\text{leg}}^{ji}\mathbf{V}_s(\theta_6^{ji},\ldots,\theta_{11}^{ji})\mathbf{V}_{r3,r4}(q_3^{ji},q_4^{ji})\mathbf{T}_{\text{tool-spa}}^{ji}\end{aligned} \tag{14}$$

with $i = 1, 2$ and $j = 1, 2$.

In the rigid case, the virtual joint coordinates θ_k^{ji} (with $k = 0\ldots11$) are equal to zero. The passive joint coordinates are

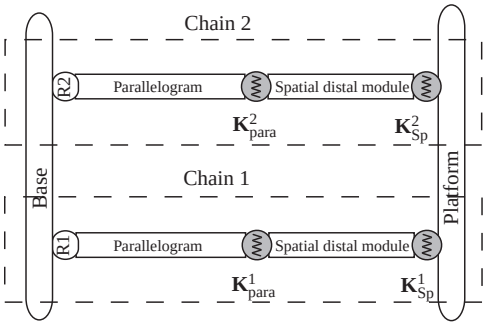

FIGURE 11. ELASTOSTATIC MODEL OF THE IRSBOT-2.

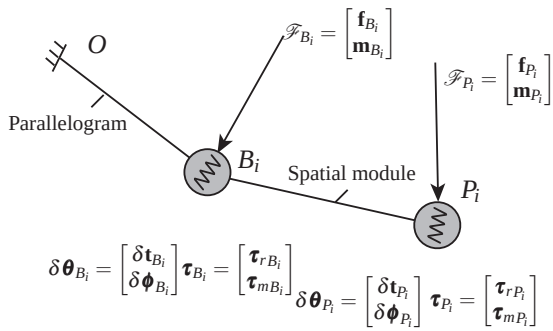

FIGURE 12. FLEXIBLE MODELLING OF THE LEG i OF THE IRSBOT-2.

obtained through the inverse kinematic model and each part of Eqn. (14) that can be derived using standard techniques for homogeneous transformation matrix.

As shown in [27], the matrix $\mathbf{J}^{ji}_{\theta}$ is obtained from the differentiation of the previous homogeneous transformation matrix $\mathbf{T}^{ji}_{\text{chain}}$ with respect to each spring parameter θ^{ji}_k:

$$\frac{\partial \mathbf{T}^{ji}_{\text{chain}}}{\partial \theta^{ji}_k} = \mathbf{H}^L_k \frac{\partial \mathbf{V}_{\theta^{ji}_k}}{\partial \theta^{ji}_k}\left(\theta^{ji}_k\right)\mathbf{H}^R_k = \begin{bmatrix} 0 & -\phi'_{iz} & \phi'_{iy} & P'_{ix} \\ \phi'_{iz} & 0 & -\phi'_{ix} & P'_{iy} \\ -\phi'_{iy} & \phi'_{ix} & 0 & P'_{iz} \\ 0 & 0 & 0 & 0 \end{bmatrix} \tag{15}$$

where $\mathbf{H}^L_k$ and $\mathbf{H}^R_k$ are constant transformation matrices with respect to the displacement θ^{ji}_k and $\partial \mathbf{V}_{\theta^{ji}_k}/\partial \theta^{ji}_k\left(\theta^{ji}_k\right)$ corresponds to the derivative of the elementary translation or rotation related to θ^{ji}_k. In (15), the terms P'_{ix}, P'_{iy}, P'_{iz} (ϕ'_{ix}, ϕ'_{iy}, ϕ'_{iz}, resp.) correspond to the small displacements of the end-effector due to the variations in the parameter θ^{ji}_k. Therefore, the k-th column of $\mathbf{J}^{ji}_{\theta}$ takes the form:

$$\left[\mathbf{J}^{ji}_{\theta}\right]_k = \left[P'_{ix}\ P'_{iy}\ P'_{iz}\ \phi'_{ix}\ \phi'_{iy}\ \phi'_{iz}\right]^T \tag{16}$$

Likewise, $\mathbf{J}^{ji}_q$ is obtained upon differentiation with respect to the passive joint coordinates q^{ji}_m (with $m = 1\ldots4$).

Once $\mathbf{J}^{ji}_{\theta}$, $\mathbf{J}^{ji}_q$ and $\mathbf{K}^{ji}_{\theta}$ are computed, it is possible to determine the stiffness matrix of each sub-chain ji using Eqn. (11) and the global stiffness matrix of the spatial distal module i denoted $\mathbf{K}^i_{\text{sp}}$ using Eqn. (13). Finally, it is possible to model each leg of the IRSBot-2 as described in Fig. 11.

It appears that the rank of $\mathbf{K}^i_{\text{sp}}$ is equal to 4 while its size is 6×6, therefore it is not invertible. However, as Eqn. (11) requires the inverse of $\mathbf{K}^i_{\text{sp}}$, using the previous presented approach for computing the global stiffness matrix of one leg is not possible. As a result, we use the following method.

Let us consider the i-th chain depicted in Fig. 12. The parallelogram is modelled as a rigid link followed by a localized spring in B_i of equivalent stiffness $\mathbf{K}^i_{\text{para}}$. Then, the spatial distal module is modelled as a rigid link followed by a localized spring in P_i of equivalent stiffness matrix $\mathbf{K}^i_{\text{sp}}$. Let $\boldsymbol{\ell}$ be the Cartesian coordinates of vector $\overrightarrow{B_iP_i}$ with $\boldsymbol{\ell} = [x,\ y,\ z]^T$.

- $\delta\mathbf{Q}_k = [\delta\mathbf{q}_k, \delta\boldsymbol{\omega}_k]^T$ denotes the small displacement screw of node k, $\delta\mathbf{q}_k$ being the small translational screw and $\delta\boldsymbol{\omega}_k$ the small rotational screw and $k = \{B_i, P_i\}$.
- $\delta\boldsymbol{\theta}_k = [\delta\mathbf{t}_k, \delta\boldsymbol{\phi}_k]^T$ is the small deflection screw of 6-dimensional spring localized at node k, $\delta\mathbf{t}_k$ being the translational deflection screw and $\delta\boldsymbol{\phi}_k$ the rotational deflection screw.
- $\boldsymbol{\tau}_k = [\boldsymbol{\tau}_{rk}, \boldsymbol{\tau}_{mk}]^T$ is the vector of the internal virtual joint wrench, with $\boldsymbol{\tau}_{rk}$ the force and $\boldsymbol{\tau}_{mk}$ the torque.
- $\mathscr{F}_k = [\mathbf{f}_k, \mathbf{m}_k]^T$ is the virtual wrench exerted on the node k, with $\mathbf{f}_k$ the force and $\mathbf{m}_k$ the torque.

The small displacements $\delta\mathbf{Q}^i$ of points B_i and P_i are related to the small deflections of springs $\delta\boldsymbol{\theta}^i_{B_i}$ and $\delta\boldsymbol{\theta}^i_{P_i}$ in each node by:

$$\delta\mathbf{Q}^i = \mathbf{B}^i\delta\boldsymbol{\theta}_i \text{ with } \delta\mathbf{Q}^i = \begin{bmatrix} \delta\mathbf{Q}_{B_i} \\ \delta\mathbf{Q}_{P_i} \end{bmatrix}, \delta\boldsymbol{\theta}^i = \begin{bmatrix} \delta\boldsymbol{\theta}_{B_i} \\ \delta\boldsymbol{\theta}_{P_i} \end{bmatrix}, \text{ and}$$
$$\mathbf{B}^i = \left[\begin{array}{cc|c} \multicolumn{2}{c|}{\mathbf{I}_{d6\times6}} & \mathbf{0}_{6\times6} \\ \hline \mathbf{I}_{d3\times3} & \mathbf{B}'^i & \\ \mathbf{0}_{3\times3} & \mathbf{I}_{d3\times3} & \mathbf{I}_{d6\times6} \end{array}\right],\ \mathbf{B}'^i = \begin{bmatrix} 0 & z & -y \\ -z & 0 & x \\ y & -x & 0 \end{bmatrix} \tag{17}$$

The internal virtual spring wrench $\boldsymbol{\tau}^i$ at B_i and P_i are related to the virtual wrench exerted $\mathscr{F}_{B_i}$ and $\mathscr{F}_{P_i}$ on each node by:

$$\boldsymbol{\tau}^i = \mathbf{A}^i\mathscr{F}^i, \text{ with } \boldsymbol{\tau}^i = \begin{bmatrix} \boldsymbol{\tau}_{B_i} \\ \boldsymbol{\tau}_{P_i} \end{bmatrix}, \mathscr{F}^i = \begin{bmatrix} \mathscr{F}_{B_i} \\ \mathscr{F}_{P_i} \end{bmatrix} \text{ and } \mathbf{A}^i = \mathbf{B}^{iT} \tag{18}$$

Finally, the small deflections of spring $\delta\boldsymbol{\theta}_i$ are related to the internal virtual spring wrench $\boldsymbol{\tau}^i$ by:

$$\boldsymbol{\tau}^i = \mathbf{K}^i_{\theta}\delta\boldsymbol{\theta}_i \text{ with } \mathbf{K}^i_{\theta} = \begin{bmatrix} \mathbf{K}^i_{\text{para}} & 0 \\ 0 & \mathbf{K}^i_{\text{sp}} \end{bmatrix} \tag{19}$$

It is possible to rearrange equations (17), (18) and (19) to obtain a relation between the external wrench and the small displacement screw of nodes $\delta\mathbf{Q}^i$:

$$\begin{bmatrix}\mathscr{F}_{B_i}\\ \mathscr{F}_{P_i}\end{bmatrix} = \mathbf{K}^i_{eq}\begin{bmatrix}\delta\mathbf{Q}_{B_i}\\ \delta\mathbf{Q}_{P_i}\end{bmatrix}, \text{ with } \mathbf{K}^i_{eq} = \mathbf{A}^{i^{-1}}\mathbf{K}^i_\theta\mathbf{B}^{i^{-1}} = \begin{bmatrix}\mathbf{k}^i_{11} & \mathbf{k}^i_{12}\\ \mathbf{k}^i_{21} & \mathbf{k}^i_{22}\end{bmatrix} \tag{20}$$

The stiffness matrix of the entire leg i linking the end-effector displacement screw $\delta\mathbf{Q}_{P_i}$ to the external wrench $\mathscr{F}_{P_i}$ exerted on the platform is given by:

$$\mathscr{F}_{P_i} = \mathbf{K}_{tot_i}\delta\mathbf{Q}_{P_i} \text{ with } \mathbf{K}_{tot_i} = -\mathbf{k}^i_{21}{\mathbf{k}^i_{11}}^{-1}\mathbf{k}^i_{12} + \mathbf{k}^i_{22} \tag{21}$$

Finally, the stiffness matrix of the entire robot, $\mathbf{K}_{tot}$, is the sum of $\mathbf{K}_{tot_1}$ and $\mathbf{K}_{tot_2}$, which allows for the computation of the end-effector small displacement screw in all configurations of the IRSBot-2.

Comparison of the IRSBot-2, Par2 and $\underline{R}RRR\underline{R}$ mechanisms

This section aims to compare the $\underline{R}RRR\underline{R}$, Par2 and IRSBot-2 robots. The design parameters of the Par2 and the $\underline{R}RRR\underline{R}$ are defined in [19]. In order to deal with equivalent kinematic performances for the IRSBot-2 and the $\underline{R}RRR\underline{R}$ mechanism defined in [19], the design parameters of the IRSBot-2 are the following: $l_1 = 0.375$ m, $l_{2eq} = 0.825$ m, $b = 0.1375$ m and $p = 0.05$ m (c.f. Fig. 5). The cross section of the cylindrical tube are defined in [19]. $D_{\text{para}} = 0.06$ m and $d_{\text{para}} = 0.05$ m are the outer and inner diameters of the proximal bar for the Par2 and the $\underline{R}RRR\underline{R}$ robots, and of the elements 1_i for the IRSBot-2 (Fig. 2).

Once these parameters are fixed, the value of the other parameters of the IRSBot-2 have to be found, i.e., d, the small side length of the parallelogram and a_1, a_2 and β defined in the page 4 as the distal module parameters (see Fig. 5). D_{parp} and d_{parp} denote the outer and inner diameters of tube 2_i, D_{sp} and d_{sp} denote the outer and inner diameters of tube 5_{ji} and D_{elbow}, d_{elbow} those of parts composing the elbow.

In order to find the optimal values for these parameters, the following optimization problem is solved:

$$P: \left|\begin{array}{ll} \text{minimize} & \mathrm{m}_{IRS}(\mathbf{x},\mathbf{p}),\\ \text{over} & \mathbf{x}\\ \text{subject to} & [\delta_{y_{IRS}}(\mathbf{x},\mathbf{p})]_{Max} < [\delta_{y_{\underline{R}RRR\underline{R}}}(\mathbf{p})]_{Max},\\ & [\delta_{y_{IRS}}(\mathbf{x},\mathbf{p})]_{Mean} < [\delta_{y_{\underline{R}RRR\underline{R}}}(\mathbf{p})]_{Mean}, \end{array}\right. \tag{22}$$

where $\mathrm{m}_{IRS}(\mathbf{x},\mathbf{p})$ is the IRSBot-2's mass, $\delta_{y_{IRS}}(\mathbf{x},\mathbf{p})$ is the deflection along $\mathbf{y}_0$ of its moving platform geometric center, $\delta_{y_{\underline{R}RRR\underline{R}}}(\mathbf{p})$ is the deflection along $\mathbf{y}_0$ of the moving platform geometric center of the $\underline{R}RRR\underline{R}$ mechanism, $\mathbf{p} = [x, z, q_1, q_2, l_1, l_{2eq}, b, p, D_{\text{para}}, d_{\text{para}}]$ is the vector of design parameters that are common to the three studied manipulators and $\mathbf{x} = [d, a_1, a_2, \beta, D_{\text{parp}}, d_{\text{parp}}, D_{\text{sp}}, d_{\text{sp}}, D_{\text{elbow}}, d_{\text{elbow}}]$ is the decision vector of the optimization problem.

TABLE 1. TOTAL MASS AND DEFLECTION FOR A 100N FORCE APPLIED ON THE END-EFFECTOR ALONG THE $\mathbf{y}_0$-AXIS FOR THE $\underline{R}RRR\underline{R}$ AND THE PAR2 ROBOTS.

Robot	Mass [Kg]	$\delta_{y_{Max}}$ [mm]	$\delta_{y_{Mean}}$ [mm]	σ_{δ_y} [mm]
$\underline{R}RRR\underline{R}$	5.6	1.227	1.135	0.064
Par2	5.77	1.158	0.382	0.205

TABLE 2. OPTIMUM DECISION VARIABLES $\mathbf{x}$ [m].

Parameters [m]								
a_2	a_1	D_{parp}	d_{parp}	D_{sp}	d_{sp}	d	D_{elbow}	d_{elbow}
0.03	0.42	0.06	0.054	0.046	0.044	0.2	0.1	0.09

TABLE 3. TOTAL MASS AND DEFLECTION FOR A 100N-FORCE APPLIED ON THE END-EFFECTOR ALONG $\mathbf{y}_0$-AXIS FOR THE IRSBOT-2.

Mass [Kg]	$[\delta_{y_{IRS}}]_{Max}$ [mm]	$[\delta_{y_{IRS}}]_{Mean}$ [mm]	$\sigma_{\delta_{y_{IRS}}}$ [mm]
10.56	1.222	0.941	0.129

In order for the comparison to be fair, the optimization problem is solved in the common Cartesian workspace, $\mathscr{W}_c$, for the three robots. The deflections of the three robots are evaluated throughout the Par2 robot workspace as the latter is the smallest one. For a given wrench applied on the end-effector its displacements of the end-effector of the three robots along the normal to their plane motion are evaluated.

For twenty configurations, the results in terms of (i) the maximal, mean and standard deviation of the deformation along $\mathbf{y}_0$ for a 100N force applied on the end-effector, and (ii) the total mass, are given in Tab. 1 for the $\underline{R}RRR\underline{R}$ and the Par2 robots. It is noteworthy that for equivalent masses, the Par2 robot is about three times stiffer than the $\underline{R}RRR\underline{R}$ robot but its standard deviation is higher.

A set of parameters for the IRSBot-2 that is close to the optimum with regard to the optimization problem is found[3] (Tab. 2). For this set of parameters, the results obtained in twenty configurations, in terms of deflection and total mass, are shown in Tab. 3.

The results show that, for equal deformations, the IRSBot-2 is bulkier than the $\underline{R}RRR\underline{R}$ mechanism.

A deeper robot analysis shows that the parallelogram rotates around the $\mathbf{x}_0$-axis under the force applied on the moving plat-

[3]This problem was solved by trial and error.

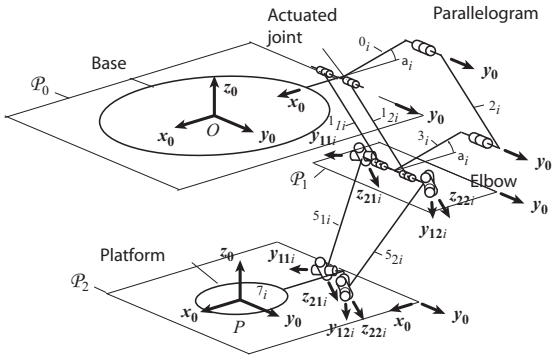

FIGURE 13. SCHEMATIC OF THE REDESIGNED IRSBOT-2.

TABLE 4. OPTIMUM DECISION VARIABLES **x** [m] AFTER REDESIGN.

a_2	a_1	D_{parp}	d_{parp}	D_{sp}	d_{sp}
0.03	0.42	0.045	0.043	0.0555	0.0535
D_{elbow}	d_{elbow}	D_{para}	d_{para}	d	
0.0285	0.026	0.049	0.0415	0.1	

TABLE 5. TOTAL MASS AND DEFLECTION FOR A 100N-FORCE APPLIED ON THE END-EFFECTOR ALONG THE $\mathbf{y}_0$-AXIS FOR THE REDESIGNED IRSBOT-2.

Mass [Kg]	$[\delta_{y_{IRS}}]_{Max}$ [mm]	$[\delta_{y_{IRS}}]_{Mean}$ [mm]	$\sigma_{\delta_{y_{IRS}}}$ [mm]
4.48	0.576	0.546	0.03

form. However an angular displacement of the parallelogram induces a large displacement of the ends of the elbow, and hence an even larger displacement of the end-effector. Consequently, a new design of the IRSBot-2 is illustrated in Fig. 13 to overcome those issues.

To minimize the rotational deflections at the end of the parallelogram, several solutions are possible, but the simplest one is to replace the element 1_i of the parallelogram by two parallel bars 1_{1i} and 1_{2i}, as depicted in Fig. 13. The further these bars are from each other, the better the elbow behaves with regard to rotational displacements.

The new design is optimized by solving the optimization problem (22). Since the number of bars is doubled to replace element 1_i, the new decision variables D_{para} and d_{para}, which are the outer and inner diameters of the cylindrical tubes forming the elements 1_{1i} et 1_{2i} are added in the optimization process.

The new set of parameters of the IRSBot-2 is given in Tab. 4 and the results obtained in terms of deflection and total mass are detailed in Tab. 5.

Figure 14 illustrates the deflection of the robots end-effector

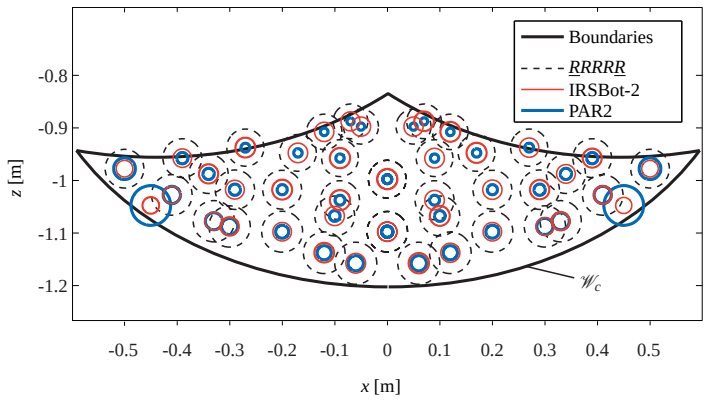

FIGURE 14. DEFLECTION OF THE – IRSBOT-2, THE – PAR2 and the - - RRRRR MECHANISM FOR SOME POSES OF THEIR END-EFFECTOR.

for different poses. The deflections are proportional to circle radii, namely,

$$r = \frac{\delta_y}{25\,\text{Max}(\delta_{y_{IRS}}, \delta_{y_{\underline{R}RRR\underline{R}}}, \delta_{y_{PAR2}})}. \tag{23}$$

From Tab. 5 and Fig. 14, the IRSBot-2 is lighter and twice stiffer than the $\underline{R}RRR\underline{R}$ mechanism under study. Moreover, as shown in Tab. 1 and Tab. 5, the variation in the deflection throughout $\mathscr{W}_c$ is smaller for the IRSBot-2 than for its two counterparts.

CONCLUSION

In this paper, a new 2-DOF translational parallel robot for high speed operations named the IRSBot-2 was presented. This robot has the following characteristics:

(i) Like the Par2, it has a spatial architecture, in which the distal parts of the legs are subject to traction/compression/torsion only. As a result, its stiffness is increased and its total mass can be reduced.

(ii) It is composed of only two legs in order to reduce the robot complexity and to increase the size of its Cartesian workspace.

Its kinematic and velocity models were developed and its singularities were analysed. An elastostatic analysis of the IRSBot-2 showed its advantages in terms of mass in motion and stiffness with respect to the Par2 robot and the $\underline{R}RRR\underline{R}$ mechanism. As a matter of fact, the IRSBot-2 turns out to be lighter than the Par2 robot and the $\underline{R}RRR\underline{R}$ mechanism, whereas its stiffness is higher than the stiffness of the $\underline{R}RRR\underline{R}$ mechanism.

It should be mentioned that a patent of the IRSBot-2 is pending. Finally, a deeper analysis of the constraint singularities of the IRSBot-2 as well as a rigorous solving of its design optimization problem are part of the future works.

References

[1] Clavel, R., 1990. Device for the movement and positioning of an element in space. Patent US 4976582, December 11.

[2] Bonev, I., 2001. Delta Parallel Robot - The Story of Success. Parallemic website. `http://www.parallemic.org/Reviews/Review002.html`.

[3] Angeles, J., Caro, S., Khan, W., and Morozov, A., 2006. "Kinetostatic design of an innovative schonflies-motion generator". Proceedings of IMechE Part C: Journal of Mechanical Engineering Science, **220** (7) Jan. , pp. 935–943.

[4] Campos, L., Bourbonnais, F., Bonev, I. A., and Bigras, P., 2010. "Development of a five-bar parallel robot with large workspace". In ASME 2010 International Design Engineering Technical Conferences.

[5] `http://www/mitsubishi-automation.fr/produts/robots_RP.html`.

[6] `http://backoffice.elau.de/files/3932_20412844/ETIE222_00_18_10_07.pdf`.

[7] `http://fanucrobotics.fr/fr/Countries/FRFR/News/M3iA.aspx`.

[8] Chablat, D., and Wenger, P., 2003. "Architecture optimization of a 3-dof translational parallel mechanism for machining applications, the orthoglide". Robotics and Automation, IEEE Transactions on, **19** (3) , pp. 403 – 410.

[9] Company, O., 2000. *Machines-outils rapides à structure parallèle. Méthodologie de conception, applications et nouveaux concepts.* PhD thesis, Université Montpellier II.

[10] Pierrot, F., Shibukawa, T., and Morita, K., 2001. Four-degree-of-freedom parallel robot. Patent EP 1 084 802 A2.

[11] Krut, S., Nabat, V., Company, O., and Pierrot, F., 2004. "A high-speed parallel robot for scara motions". In Robotics and Automation, 2004. Proceedings. ICRA '04. 2004 IEEE International Conference on, vol. 4, pp. 4109 – 4115.

[12] Company, O., Pierrot, F., Nabat, V., and de la O Rodriguez, M., 2005. "Schoenflies motion generator: A new non redundant parallel manipulator with unlimited rotation capability". In Robotics and Automation, 2005. ICRA 2005. Proceedings of the 2005 IEEE International Conference on, pp. 3250 – 3255.

[13] Nabat, V., Pierrot, F., de la O Rodriguez Mijangos, M., Azcoita Arteche, J. M., Bueno Zabalo, R., Company, O., and Florentino Perez De Armentia, K., 2007. High-speed parallel robot with four degrees of freedom. Patent EP 1 870 214 A1.

[14] Brogardh, T., 2001. Device for relative movement of two elements. Patent US 6301988 B1.

[15] Liu, X., and Kim, J., 2002. "Two novel parallel mechanisms with less than six degrees of freedom and the applications". In Proc. Workshop on Fundamental Issues and Future Reserch Directions for Parallel Mechanisms and Manipulators, pp. 172–177.

[16] Huang, T., Li, M., Li, Z., Chetwynd, D., and Whitehouse, D., 2003. Planar parallel robot mechanism with two translational degrees of freedom. Patent WO 03055653 A1.

[17] Caro, S., Khan, W. A., Pasini, D., and Angeles, J., 2010. "The rule-based conceptual design of the architecture of serial schönflies-motion generators". Mechanism and Machine Theory, **45** (2) Feb. , pp. 251–260.

[18] Pierrot, F., Sébastien, K., Olivier, C., Vincent, N., Cédric, B., and A., S. F., 2009. Two degree-of-freedom parallel manipulator. Patent WO 2009/089916 A1.

[19] Pierrot, F., Baradat, C., Nabat, V., Company, O., Krut, S., and Gouttefarde, M., 2009. "Above 40g acceleration for pick-and-place with a new 2-dof pkm". In Robotics and Automation, 2009. ICRA '09. IEEE International Conference on, pp. 1794 –1800.

[20] Liu, X.-J., Wang, J., and Pritschow, G., 2006. "Kinematics, singularity and workspace of planar 5r symmetrical parallel mechanisms". Mechanism and Machine Theory, **41** (2) , pp. 145 – 169.

[21] Chablat, D., and Wenger, P., 2001. "Séparation des solutions aux modèles géométriques direct et inverse pour les manipulateurs pleinement parallèles". Mechanism and Machine Theory, **36** (6) , pp. 763–783.

[22] Gosselin, C., and Angeles, J., 1990. "Singularity analysis of closed-loop kinematic chains". Robotics and Automation, IEEE Transactions on, **6** (3) June , pp. 281 –290.

[23] Merlet, J.-P., 2006. *Parallel Robots, Second Edition*, vol. 128. Springer.

[24] Zlatanov, D., Bonev, I., and Gosselin, C., 2002. "Constraint singularities of parallel mechanisms". In Robotics and Automation, 2002. Proceedings. ICRA '02. IEEE International Conference on, vol. 1, pp. 496 – 502.

[25] Amine, S., Kanaan, D., Caro, S., and Wenger, P., 2010. "Constraint and singularity analysis of lower-mobility parallel manipulators with parallelogram joints". In ASME 2010 International Design Engineering Technical Conferences.

[26] Germain, C., 2010. Analyse et conception d'un nouveau manipulateur parallèle à deux degrès de liberté pour des applications de pick-and-place. Master's thesis, Ecole Centrale de Nantes, Septembre. See also URL `http://www.irccyn.ec-nantes.fr/~germain`.

[27] Pashkevich, A., Chablat, D., and Wenger, P., 2009. "Stiffness analysis of overconstrained parallel manipulators". Mechanism and Machine Theory, **44** (5) , pp. 966 – 982.

[28] Pashkevich, A., Klimchik, A., Caro, S., and Chablat, D., 2010. "Stiffness modelling of parallelogram-based parallel manipulators". *New Trends in Mechanism Science, Analysis and Design, Springer Eds* , pp. 675–682.